Digital holography as 3D tracking tool for assessing acoustophoretic particle manipulation

T. CACACE,[1,2,*] M. PATURZO,[1] P. MEMMOLO,[1,3] M. VASSALLI,[4] P. FERRARO,[4] M. FRALDI,[5] AND G. MENSITIERI[6]

[1]*National Research Council of Italy, Institute of Applied Sciences and Intelligent Systems 'E. Caianiello', Via Campi Flegrei 34, Pozzuoli, Naples, Italy*
[2]*Department of Mathematics and Physics, University of Campania "L. Vanvitelli", Viale Lincoln 5, 81100, Caserta, Italy*
[3]*Currently at CNR - Institute for Microelectronics and Microsystems, Unit of Naples, via P. Castellino 111 80131 Naples, Italy*
[4]*National Research Council of Italy, Institute of Biophysics, Via De Marini 6, 16149 Genova, Italy*
[5]*Department of Structures for Engineering and Architecture, University of Naples Federico II, Piazzale Tecchio 80, 80125 Naples, Italy*
[6]*Department of Chemical, Materials and Production Engineering University of Naples Federico II, Piazzale Tecchio 80, 80125 Naples, Italy*
[*]t.cacace@isasi.cnr.it

Abstract: The integration of digital holography (DH) imaging and the acoustic manipulation of micro-particles in a microfluidic environment is investigated. The ability of DH to provide efficient 3D tracking of particles inside a microfluidic channel is exploited to measure the position of multiple objects moving under the effect of stationary ultrasound pressure fields. The axial displacement provides a direct verification of the numerically computed positions of the standing wave's node, while the particle's transversal movement highlights the presence of nodes in the planar direction. Moreover, DH is used to follow the aggregation dynamics of trapped spheres in such nodes by using aggregation rate metrics.

References and links

1. M. Evander and J. Nilsson, "Acoustofluidics 20: Applications in acoustic trapping," Lab Chip **12**(22), 4667–4676 (2012).
2. C. R. P. Courtney, C. K. Ong, B. W. Drinkwater, P. D. Wilcox, C. Demore, S. Cochran, P. Glynne-Jones, and M. Hill, "Manipulation of microparticles using phase-controllable ultrasonic standing waves," J. Acoust. Soc. Am. **128**(4), EL195–EL199 (2010).
3. G. Sitters, D. Kamsma, G. Thalhammer, M. Ritsch-Marte, E. J. G. Peterman, and G. J. L. Wuite, "Acoustic force spectroscopy," Nat. Methods **12**(1), 47–50 (2014).
4. C. W. Shields IV, C. D. Reyes, and G. P. López, "Microfluidic cell sorting: a review of the advances in the separation of cells from debulking to rare cell isolation," Lab Chip **15**(5), 1230–1249 (2015).
5. P. Mishra, M. Hill, and P. Glynne-Jones, "Deformation of red blood cells using acoustic radiation forces," Biomicrofluidics **8**(3), 034109 (2014).
6. J. Y. Hwang, J. Kim, J. M. Park, C. Lee, H. Jung, J. Lee, and K. K. Shung, "Cell deformation by single-beam acoustic trapping: a promising tool for measurements of cell mechanics," Sci. Rep. **6**(1), 27238 (2016).
7. M. Fraldi, A. Cugno, L. Deseri, K. Dayal, and N. M. Pugno, "A frequency-based hypothesis for mechanically targeting and selectively attacking cancer cells," J. R. Soc. Interface **12**(111), 20150656 (2015).
8. M. Fraldi, A. Cugno, A. R. Carotenuto, A. Cutolo, N. M. Pugno, and L. Deseri, "Small-on-Large Fractional Derivative–Based Single-Cell Model Incorporating Cytoskeleton Prestretch," J. Eng. Mech. **143**(5), D4016009 (2017).
9. A. Lamprecht, S. Lakämper, T. Baasch, I. A. T. Schaap, and J. Dual, "Imaging the position-dependent 3D force on microbeads subjected to acoustic radiation forces and streaming," Lab Chip **16**(14), 2682–2693 (2016).
10. J. V. Oever, R. Frentrop, D. Wijnperlé, H. Offerhaus, D. van den Ende, J. Herek, and F. Mugele, "Imaging local acoustic pressure in microchannels," Appl. Opt. **54**(21), 6482–6490 (2015).
11. R. Barnkob, P. Augustsson, T. Laurell, and H. Bruus, "Measuring the local pressure amplitude in microchannel

acoustophoresis," Lab Chip **10**(5), 563–570 (2010).

12. P. B. Muller, M. Rossi, Á. G. Marín, R. Barnkob, P. Augustsson, T. Laurell, C. J. Kähler, and H. Bruus, "Ultrasound-induced acoustophoretic motion of microparticles in three dimensions," Phys. Rev. E Stat. Nonlin. Soft Matter Phys. **88**(2), 023006 (2013).

13. R. Barnkob, C. J. Kähler, M. Rossi, H. Bruus, and R. Adrian, "General defocusing particle tracking," Lab Chip **15**(17), 3556–3560 (2015).

14. D. Kamsma, R. Creyghton, G. Sitters, G. J. L. Wuite, and E. J. G. Peterman, "Tuning the Music: Acoustic Force Spectroscopy (AFS) 2.0," Methods **105**, 26–33 (2016).

15. M. K. Kim, "Principles and techniques of digital holographic microscopy," SPIE Rev. **1**, 18005 (2010).

16. P. Memmolo, L. Miccio, M. Paturzo, G. Di Caprio, G. Coppola, P. A. Netti, and P. Ferraro, "Recent advances in holographic 3D particle tracking," Adv. Opt. Photonics **7**(4), 713 (2015).

17. L. Miccio, P. Memmolo, F. Merola, S. Fusco, V. Embrione, A. Paciello, M. Ventre, P. A. Netti, and P. Ferraro, "Particle tracking by full-field complex wavefront subtraction in digital holography microscopy," Lab Chip **14**(6), 1129–1134 (2014).

18. E. Meijering, O. Dzyubachyk, and I. Smal, "Methods for cell and particle tracking," Methods Enzymol. **504**, 183–200 (2012).

19. T.-W. Su, L. Xue, and A. Ozcan, "High-throughput lensfree 3D tracking of human sperms reveals rare statistics of helical trajectories," Proc. Natl. Acad. Sci. U.S.A. **109**(40), 16018–16022 (2012).

20. P. Memmolo, M. Paturzo, B. Javidi, P. A. Netti, and P. Ferraro, "Refocusing criterion via sparsity measurements in digital holography," Opt. Lett. **39**(16), 4719–4722 (2014).

21. P. Memmolo, C. Distante, M. Paturzo, A. Finizio, P. Ferraro, and B. Javidi, "Automatic focusing in digital holography and its application to stretched holograms," Opt. Lett. **36**(10), 1945–1947 (2011).

22. P. Memmolo, A. Finizio, M. Paturzo, L. Miccio, and P. Ferraro, "Twin-beams digital holography for 3D tracking and quantitative phase-contrast microscopy in microfluidics," Opt. Express **19**(25), 25833–25842 (2011).

23. P. Memmolo, M. Iannone, M. Ventre, P. A. Netti, A. Finizio, M. Paturzo, and P. Ferraro, "On the holographic 3D tracking of in vitro cells characterized by a highly-morphological change," Opt. Express **20**(27), 28485–28493 (2012).

24. F. Merola, P. Memmolo, L. Miccio, R. Savoia, M. Mugnano, A. Fontana, G. D'ippolito, A. Sardo, A. Iolascon, A. Gambale, and P. Ferraro, "Tomographic flow cytometry by digital holography," Light Sci. Appl. **6**, e16241 (2016).

25. V. Bianco, B. Mandracchia, V. Marchesano, V. Pagliarulo, F. Olivieri, S. Coppola, M. Paturzo, and P. Ferraro, "Endowing a plain fluidic chip with micro-optics: a holographic microscope slide," Light Sci. Appl. **6**, e17055 (2017).

26. X. Yu, J. Hong, C. Liu, and M. K. Kim, "Review of digital holographic microscopy for three-dimensional profiling and tracking," Opt. Eng. **53**(11), 112306 (2014).

27. D. Kamsma and G. Sitters, "AFS 1D model.figshare," https://dx.doi.org/10.6084/m9.figshare.3166753.v1.

28. R. J. Townsend, M. Hill, N. R. Harris, and N. M. White, "Investigation of two-dimensional acoustic resonant modes in a particle separator," Ultrasonics **44**(Suppl 1), e467–e471 (2006).

29. M. Settnes and H. Bruus, "Forces acting on a small particle in an acoustical field in a viscous fluid," Phys. Rev. E Stat. Nonlin. Soft Matter Phys. **85**(1), 016327 (2012).

30. G. Dardikman, M. Habaza, L. Waller, and N. T. Shaked, "Video-rate processing in tomographic phase microscopy of biological cells using CUDA," Opt. Express **24**(11), 11839–11854 (2016).

31. S. M. Hagsäter, A. Lenshof, P. Skafte-Pedersen, J. P. Kutter, T. Laurell, H. Bruus, J. Nilsson, and S. Johansson, "Acoustic resonances in straight micro channels: Beyond the 1D-approximation," Lab Chip **8**(7), 1178–1184 (2008).

1. Introduction

Manipulation of particles in microchannels using ultrasound (US) waves, commonly known as acoustophoresis, is an effective tool for microfluidic lab-on-chip devices. Depending on the adopted geometry, the radiation forces have been successfully employed to manipulate particles promoting clusters formation [1], moving them to arbitrary positions [2], levitating or pushing them toward a surface [3] or sorting them based on their size and density [4]. Moreover, biological samples can be deformed by US [5,6] or stimulated at prescribed US frequencies to selectively induce mechanical effects [7,8]. Still, the growing complexity of geometrical configurations hinders the exact prediction of acoustic modes and resonance strength, obstructing a comprehensive development of the systems and large-scale diffusion.

Thus, not only is it important to experimentally monitor the manipulation effectiveness, but a calibration of the obtained pressure field is also required. The two matters are often connected. Indeed, apart from few example of direct force measurement [9] or particle-free pressure determination [10], most calibration strategies rely ultimately on particle tracking [11–14]. In this case, special care is needed when considering axial tracking. In the last years,

techniques like astigmatism particle tracking velocimetry and general defocusing have been introduced. The former codes the particles' depth position by optical distortions initiated by a cylindrical lens [12], while the latter recover the axial position from microscopic observation, based on the interpretation of the diffraction rings [13,14]. However, these procedures cannot be easily extended to heterogeneous samples, such as biological ones. Moreover, general defocusing relies on a substantial calibration procedure.

These limitations can be surmounted using DH in microscopy. This label-free imaging technique supplies amplitude and quantitative phase-contrast maps (QPMs) [15], allowing the investigation of dynamic processes and the 3D tracking of multiple cells and particles [16–19]. The axial displacements are evaluated by refocusing criteria [20,21], while the lateral shifts can be computed from the QPMs by conventional video-tracking methods [22,23]. The information is recovered by numerical post-processing, regardless of the particle shape, and no prior calibration is needed. Moreover, the ability to produce QPMs is fundamental for the study of transparent biological samples. From the phases, additional information on manipulated cells, such as morphology, could be extracted [24]. New DH schemes are being developed to use this technique out of the lab [25]. Hence, the application of DH in concert with acoustophoresis may lead to new ways to merge advanced manipulation and diagnostic.

In this work, we demonstrate the employment of DH to study the 3D position of polystyrene microspheres manipulated by US standing waves. We exploit a refocusing criteria based on Tamura coefficient [16,26] to monitor displacements along the optical axis. Then, we apply the centroid-based 2D tracking strategy [20] to calculate the transverse particles motion. Finally, we study the dynamic degree of particles aggregation in clusters in nodal planes by using two metrics, i.e. the number of clusters of microspheres and the number of microspheres per cluster.

2. Holographic recording and data processing

We use a Mach-Zehnder-based digital holography setup, working in transmission [Fig. 1(a)]. The emitted light of a laser (λ = 488 nm) is divided into an object wave (O) and a reference wave (R) by a 50:50 beam splitter. The former impinges orthogonally on the sample and it is coupled into a microscope objective (MO). The reference wave is guided through a second a second MO to compensate for aberrations (Fourier configuration). The two beams a recombined by a second beam splitter, slightly tilted to achieve off-axis geometry, and the resulting interferogram, is recorded by a CMOS digital camera and transferred to an image processing system for the reconstruction and the evaluation of the digital holograms.

To generate the US standing waves we employ a commercially available acoustophoresis microchip (LUMICKS) [3,14]. The device [Fig. 1(b)] consist of two glass layers with a fluid channel in between and a transparent piezo element on top, which is connected to a function generator and driven by sinusoidal signals. The producer of the acoustophoresis microchip has also furnished a software that, given the particles and medium material properties, calculates the resonance frequencies and the corresponding force profiles within the fluid layer [27]. The software employs a one-dimensional model to calculate the radiation force acting in the direction of the US wave's propagation [14]. In general, this force pushes the particles towards either the pressure nodes or antinodes, depending on their characteristics and that of the medium. In our case- polystyrene beads in water-it is expected that the particles are driven toward pressure nodes, which is in accordance with our observations. From the set of predicted resonance frequencies we have chosen two, 14.23MHz and 7.04MHz, based on the expected nodes position. The real resonances are experimentally established applying on the sample the frequencies around the predicted ones. Two strong responses, causing the dispersed microbeads to levitate ad aggregate, are found respectively at f_1 = 6.96MHz and f_2 = 14.11MHz. Fixed the resonance, the amplitude of the force scales linearly with the applied electric power. Thus, it can be easily tuned to suit ones needs [14]. It is worth to stress that the model employed is one-dimensional and does not account for the

radiation force's lateral components. They arise from lateral variations within the acoustic field, traced back to structural modes within the chamber walls, near-field effects or enclosure modes [28]. The later components promote the formation two-dimensional aggregates when the particles have reached their equilibrium plane. This process is also influenced by secondary radiation forces, caused by the sound field's scattering from the particles [29].

Our sample consist of polystyrene beads dispersed in water. The polystyrene microspheres (PS) carboxylate-modified 4% solids have diameter 5.1 μm, and their density at 20°C is of 1.055 g cm-3. Before the experimental acquisition the mixture is sonicated, then it is inserted in the microchannel and left unperturbed for about 30 min to ensure sedimentation. Then, holographic sequences of the changes in the microspheres position upon application of different US standing waves are recoded.

The study is articulated in two steps. In the first part, we demonstrate the ability of DH to track simultaneously the 3D displacement of multiple isolated particles. In the setup, a MO (20X, NA = 0.5) is mounted to enhance the DH resolution capabilities along the optical axis, while the camera acquisition rate is of 50 fps. We apply the frequencies f1 = 6.96MHz and f2 = 14.11MHz in a sequence. The two standing waves have nodal planes positioned at specific, well-separated heights, and when they are applied the microspheres move from one node to another. The piezo is driven with a peak-to-peak voltage of 4V. The signal amplitude has been chosen to minimize the impact of the lateral component of the radiation force, which tends to move the particles in the x-y plane and drive them outside the FOV. The sample holder position is initially adjusted so that the spheres are in the focal plane. Following the application of the resonance frequencies' sequence, the microspheres move towards available nodes, changing their axial position, and the acquired images became out-of-focus.
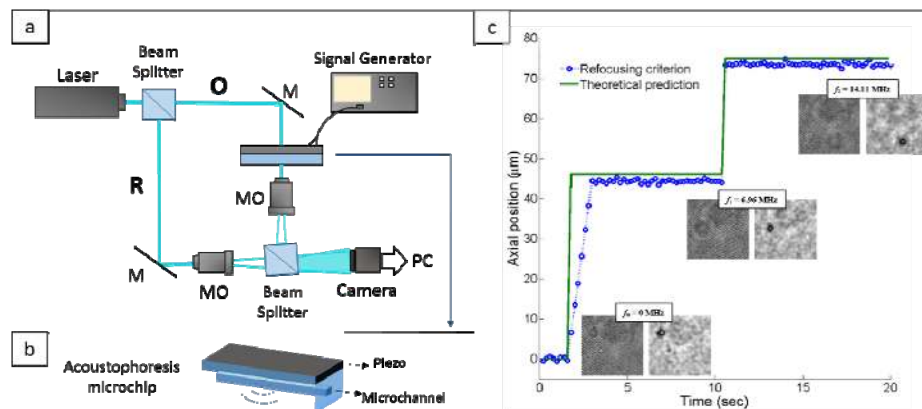

Fig. 1. (a) Mach-Zehnder setup for DH microscopy in transmission mode. Laser (λ = 488nm); O: object wave; R: reference wave; M: mirror; MO: microscope objective; Camera: CMOS image sensor. (b) Flow cell's structure. It consists of two glass plates with a fluid chamber in between. A transparent piezo plate is attached on top and connected to a signal generator. (c) Changes in the experimental particle's axial position upon application of two resonant frequencies, 6,96MHz and 14.11MHz, compared to the theoretical model. The inset images show the recorded holograms (left) and the in-focus amplitude reconstructions (right), calculated by using Tamura refocusing.

Moreover, the particles change their position in the transverse plane under the action of lateral components of the force. For each video frame, which is a holographic image of the sample, the 3D particles' position is recovered numerically, reconstructing their movement over the entire experiment. The 3D tracking strategy is articulated in two steps, i.e. automatic refocusing to recover the particles axial position and a transverse displacements estimation methods [14]. In particular, we employ a contrast-based refocusing criterion [20,21], called Tamura coefficient, defined as $T_d = \sqrt{\sigma(\mathrm{A}_d)/\mu(\mathrm{A}_d)}$, where A_d is the amplitude

reconstruction of the digital hologram calculated at distance d, σ(•) and μ(•) are the standard deviation and average value operators, respectively. The refocusing distance d_{foc} is obtained by calculating the maximum value achieved by T_d [16]. Concerning the transverse localization, we employ the centroid-based 2D tracking strategy applied on in-focus amplitude reconstructions. In particular, we calculate the Otsu filter of each amplitude reconstruction, then centroids of all retrieved particle silhouettes are calculated [20]. In Fig. 1(c) are reported the results obtained for a single isolated particle, as exemplary case of acquisition and reconstruction of axial displacements. The microsphere initial position is taken as the reference height, i.e. the initial axial position is assumed as zero height. When the first standing wave is generated, the resulting primary acoustic radiation force traps the particle at the nearest nodal plane (at about 46 μm from the initial position). Subsequently, the 14.11MHz resonance frequency is applied and the microsphere moves towards the nearest nodal plane, placed at about 75 μm. The reconstructed axial position are reported in Fig. 1(c), along with the nodal positions calculated by the software. Notice that in the first case the microsphere needs about 1.5 sec from the instant in which the field is applied to reach the nodal plane. In the second case, the result is reached in less than a 0.2 sec. The difference is due to the different travelling distances and to the difference in the radiation force's intensity.

3. Acoustophoretic particle manipulation and 3D tracking

If the alternation of the frequencies f1 and f2 is continued, the microbeads move between the two axial nodes. This is proved analyzing the holographic sequence reported in Visualization 1. As the particles are subjected to the radiation forces for longer times, they start to move also in transverse plane. In particular, it can be observed a trend in the particles disposition along specifics lines, characteristic of the applied frequency. This last evidence is highlighted in the Visualization 1 and in Fig. 2 (last frame of Visualization 1), where four particles are simultaneous tracked in 3D. In particular we observe the particles behavior for about 80 sec, changing 7 times the frequency between f1 and f2 as reported in Fig. 2(b). Instead, Fig. 2(a) shows the 2D particles motion, highlighting the presence of multiple transversal nodes, not predicted by the theoretical simulation [14] available to us. Finally, Fig. 2(c) reports the 3D trajectories of the four tracked microspheres. Our holographic 3D tracking algorithm employs up to 40 seconds to reconstruct one frame, with a precision of 110x110x350 nm³. However, a real-time implementation of these numerical procedures is feasible [30].
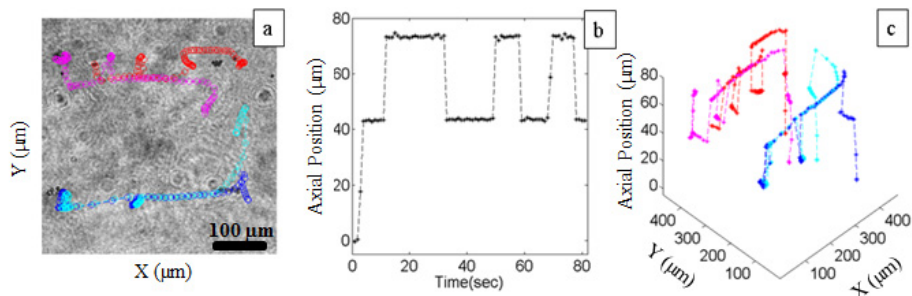

Fig. 2. Holographic 3D tracking of multiple particles by acoustic manipulation. Transversal (a) and axial (b) particles positioning under the effect of changing pressure fields generated through ultrasonic waves at frequencies f1 = 6.96 MHz and f2 = 14.11 MHz. In (c) the 3D trajectories of particles are obtained from (a,b). See Visualization 1.

The arising of 3D resonances due to the microchannel's finite dimension can be highlighted only experimentally, because the simulation, based on a one-dimensional model, doesn't account for the 3D nature of the device. Using more suitable and complex models, it would be possible to account for lateral variations in the acoustic field [28,31], predicting the existence of aggregations and particles striations across the width of the fluid layer [28].

In the second part, we study the aggregation dynamics on particles ensembles, where a single US standing wave is applied and the particles' aggregation rate is monitored. In this case, a 10X MO (NA = 0.5) is mounted to extend the FOV, guaranteeing that a significant number of particles are imaged simultaneously. The frequency 14.11MHz is applied, which results in the highest force intensities and thus has the strongest effect on the particles. The driving voltage has a 7Vpp amplitude. Following the US application, the microspheres move towards the first available node, then they start to form aggregates in the nodal plane. From the video frames the in-focus amplitude reconstruction are obtained by using the Tamura refocusing, then the aggregation rate is monitored. In particular, we analyze the particles aggregation rate by using two metrics, i.e. the number of clusters of microspheres in time and the number of microspheres per cluster in time. We apply an image segmentation method based on Otsu filter to detect single particle as well as aggregate particles. Thus, we can define separated regions of interest (ROIs), the size of which are related to a certain number of microspheres. Of course, the smallest ROI is obtained by a single particle. We define the number of clusters as the number of ROIs, while the number of microspheres per cluster is defined as the area of the corresponding ROI divide by the ideal area of one microsphere.
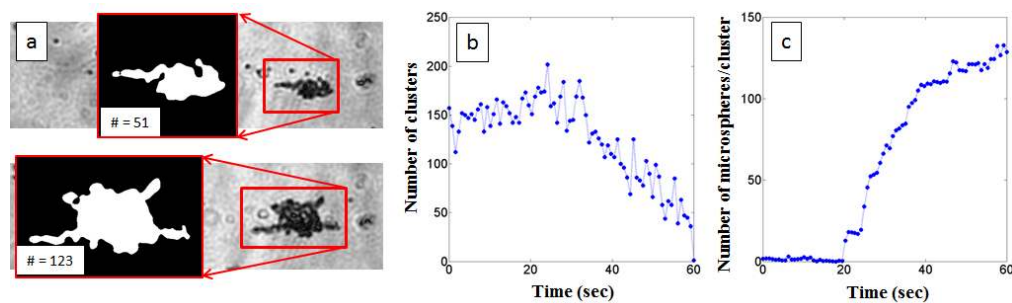

Fig. 3. (a) Two amplitude reconstructions of the holographic sequence. The red boxes highlight the results of the ROI extraction method. The estimated number of microspheres for the detected cluster is calculated. (b) Estimated number of clusters of microspheres and (c) number of microspheres per cluster in time.

In particular, in Fig. 3 the formation of a single cluster is monitored. In Fig. 3(a) we report the results of the ROI extract method applied to amplitude reconstructions of a hologram sequence, while in Figs. 3(b) and 3(c) the two plots of number of clusters/time and number of microspheres per cluster/time. We report the observation of the particles aggregation over a time interval of about 60 s, which is the time needed for this cluster to stabilize. It can be seen that while initially about 150 clusters are present (which are isolated particles), after 60 seconds only one cluster remain, resulting from the aggregation of all of those present. Note that the number of cluster seems to increase in the time interval between 20 and 30 seconds. This happen as new particles, initially outside the region of interest, enter it. The same measurement is repeated for all clusters in the FOV, achieving an aggregation time no longer than 70 seconds with a number of particles per cluster in the range 100-150.

4. Conclusions

In this work, we employed DH imaging to track the 3D position of microparticles subjected to acoustic manipulation in a microfluidic chip. The ability to monitor particle's position has been verified in two different regimes. Initially, to highlight the evaluation of 3D displacements, two different US standing waves have been alternated in the microchannel. The subsequent changes in particles heights have been successfully followed by DH, and the experimental results agree with the numerical value from numerical simulation of the nodes position. Then, the aggregation dynamics of spheres trapped in a fixed plane is studied, exploiting numerical analysis to follow the formation of the 2D clusters and evaluating the

number of comprising particles. DH has proved to be a powerful tool to quantify the 3D position of particles manipulated by US in a microfluidic channel, and as such it could be effectively applied for calibration of the ultrasonic radiation forces. Moreover, the ability to implement real-time tracking suggest its possible application as a control tool to validate the manipulation effectiveness in lab-on-chip devices and for biological samples monitoring.

Acknowledgments